The Report Committee for Sean Michael Berg
Certifies that this is the approved version of the following report:

Constructal Trees: Micro-Fabrication Techniques and Experimental Methodology

APPROVED BY
SUPERVISING COMMITTEE:

Supervisor:

Alexandre K. da Silva

Carlos H. Hidrovo

Constructal Trees: Micro-Fabrication Techniques and Experimental Methodology

by

Sean Michael Berg, BSME

Report

Presented to the Faculty of the Graduate School of

The University of Texas at Austin

in Partial Fulfillment

of the Requirements

for the Degree of

Master of Science in Engineering

The University of Texas at Austin

December 2010

Dedication

To my family: for their love and support, and for their help in making my education possible.

Acknowledgements

I would like to express great thanks to my research advisor, Professor Alexandre K. da Silva, for all of the guidance and support he has given me throughout my research project. I greatly appreciate the financial support I received as a research assistant in his group as it allowed me to focus on conducting my research, and to finish in a timely manner. Professor da Silva's expertise and experience greatly aided in my understanding of the manner in which experimental research is conducted at the graduate and professional level. I am very thankful for Professor da Silva's intelligent and creative approach to experimental research as it was invaluable to completing this report.

Financial support was made possible by the Department of Mechanical Engineering at The University of Texas at Austin, and by Alexandre K. da Silva, Ph.D.

I would also like to thank report committee member, Professor Carlos H. Hidrovo. I am grateful for his time and efforts, and thankful to have this report reviewed by a distinguished scholar with important contributions to the field of multi-scale thermal-fluid systems.

Finally, I would like to thank Robert Hart. Robert's vast experience in research and experimental work made him a knowledgeable and valuable member of our research group. I am glad I had the opportunity to work with him, and feel that I have gained a valuable perspective in the field of research in engineering.

December 3, 2010

Abstract

Constructal Trees: Micro-Fabrication Techniques and Experimental Methodology

Sean Michael Berg, MSE

The University of Texas at Austin, 2010

Supervisor: Alexandre K. da Silva

This report discusses the use of micro-fabrication techniques for creating experimental test sections containing trees of micro-finned conducting pathways, also referred to as constructal trees, for cooling a heat generating substrate. These trees are made of copper and contain branches that bifurcate at 90˚ angles to form constructal patterns. The patterns for the finalized test sections were created using photolithography techniques, and copper was deposited via thermal evaporation onto a 1 cm^2 substrate to create the trees. Certain test section design parameters were varied including the geometric complexity of the constructal trees, the volume of copper used between tree complexities, choice of material for the substrate, and the height, or thickness, of the trees. Also described in this report is an experimental methodology and testing apparatus designed to assess the cooling performance of the test sections. This methodology includes using controlled uniform heating applied to the bottom of each test section, while cooled nitrogen is impinged on the tip of the constructal tree to create a heat sink.

Table of Contents

List of Tables

List of Figures

Chapter 1 Introduction

1.1 Motivation

The generation of heat in certain systems may cause undesired effects that lead to adverse consequences. For example, in many electronics applications, heat generation causes substrate surface temperatures to increase, which may lead to the development of thermal stresses in the substrate and, over time, can result in mechanical failure (Federov and Viskanta, 2000; Magill, 2010). Hot spots also tend to form because of the grouping of certain heat generating components within small areas of these systems, on the order of 1 cm^2, and this exacerbates the problem (Pop et al., 2006; Jacob Baker, 2008). Furthermore, the scale of operation is important to consider due to a continued push for building progressively smaller electronic packages (Moore, 1965; Schaller, 1997). It is therefore desirable to remove heat in the most efficient manner possible to enhance these system's performance and lifetime (Bejan, 1997a; Bejan, 1997b).

Since the scale of operation is very small, often on the order of 10-100 microns, the use of cooling by convection may become difficult if the ducts that carry the coolant fluid are large compared to the system (Bejan, 1997b). In these instances, cooling through conduction heat transfer would then become necessary. A number of enhanced conduction heat transfer systems have been studied in literature (Webb and Kim, 2005). The use of extended surfaces, or fins, has been the most prevalent model in computational and experimental work (Brignoni and Garimella, 1999; Culham and Muzychka, 2001). The concept of optimizing fin geometries for enhanced cooling has been explored extensively (Bejan, 1997a; Bejan, 2000). Constructal theory was proposed by A. Bejan in 1997 to address this concept, wherein it is shown analytically that there exists an optimal fin geometry for cooling in this application (Bejan, 1997b).

1.2 Bejan's Constructal Theory

The principle idea behind constructal theory is adding smaller "constructs" to a larger base structure (Bejan, 1997b). The addition of these "constructs" occurs through the bifurcation of a path into multiple smaller paths. This concept is often observed in nature through a number of geometrically branched networks which include the human vascular system, trees and leaves, and rivers (Bejan, 2000). The constructal networks proposed by Bejan, referred to as constructal trees because of their resemblance to tree-like shapes, often enhance the ability of flows to travel between two points because of the geometry of the networks (Bejan, 1997b).

1.3 Literature Review

In the interceding years since the "tree" was first proposed by Bejan in 1997, there have been a number of studies conducted that explore the concept of enhanced heat transfer using constructal trees in a variety of systems and applications. A number of these studies have been conducted by Bejan and others in this area, and several publications present results based on optimizing fin geometries for cooling in thermal systems, which confirm predictions of the original theory (Bejan, 1997c; Bejan et al., 1997; Bejan and Dan, 1999; Alebrahim and Bejan, 1999; Almogbel and Bejan, 2000).

Others have expanded on Bejan's theory by modifying the system design and exploring those effects. One such case conducted by Almogbel and Bejan in 2001 modifies the original theory by relaxing the constraint of the so-called "interstitial spacing" of each of the branches within the tree. In other words, the number of tree branches becomes denser near the edges of the substrate surface, which is where the highest temperatures are encountered. The results show an improvement in cooling performance (Almogbel and Bejan, 2001). In another case by Ledezma and Bejan in 1998, a three dimensional cylindrical system is analyzed. A composite heat generating cylinder with laterally bifurcating fibers is studied analytically and numerically (Ledezma

and Bejan, 1998). Another study conducted by Rocha et al. in 2002 analyzes a disc shaped system with a heat sink positioned at the center of the disc, where cooling in the radial direction is the focus (Rocha et al., 2002). Despite the variations, the results in each of these cases still confirm the original theory (Bejan, 1997b; Ledezma and Bejan, 1998; Almogbel and Bejan, 2001; Rocha et al., 2002).

A number of numerically based studies have also been conducted (Li et al., 2004; Gersborg-Hansen et al., 2006; Gosselin and Mathieu, 2007; Kobayashi et al., 2009). The findings from these confirm that using networks resembling constructal trees provides the most effective manner for dissipating heat in these systems, which numerically validates the original theory (Bejan, 1997b; Bejan, 2000).

1.4 Proposed Work

This report contributes to work in this field of study because, to the best of this author's knowledge, all previous work in regards to constructal trees has been purely theoretical. The primary objective for this study was to devise an experiment for evaluating the effectiveness of constructal trees for cooling. A suitable method for depositing the constructal trees onto a substrate was determined in order to create the test sections required for the experiment. Furthermore, devising a methodology and building an experimental apparatus capable of measuring the cooling performance of the fabricated test sections was necessary. The conclusions in this report will provide a basis for assessing the effectiveness of constructal trees experimentally by including recommendations for creating test sections, and a metric for measuring the cooling performance of these thermal systems.

A variety of micro-fabrication techniques were tested in order to determine the most effective method for creating the experimental test sections. The design of the test sections for the experiment warrant careful consideration since a number of parameters can affect the cooling performance of the system. These include the choice of substrate

material, and the dimensions of the constructal trees, i.e. width and height of the tree branches. By varying each of these parameters during the fabrication process, the extent of each effect can eventually be measured through experiment.

Substrate materials were explored during the micro-fabrication process. Silicon and glass substrates were chosen for their very different thermal conductivities (Incropera et al., 2006). Copper was selected as the material for the constructal tree because of its high thermal conductivity (Incropera et al., 2006). Since the thermal conductivity of glass is very low compared to that of copper and silicon, it is thought that the cooling effects might be magnified for those test sections with glass substrates (Bejan, 1997b; Bejan, 2000).

It was also desired to assess the extent to which the tree dimensions affected cooling performance. The surface area of the trees was one aspect, where in one case the tree surface area for each individual test section was unconstrained and varied with tree geometric complexity. In other words, the surface area of the tree increased as the geometric complexity of the tree increased. The other case involved constraining the surface area of the trees for all complexities. In addition, varying the height of the trees was also done. This was particularly important because it was proposed in the original theory that the height of the trees should be "small" compared to the other dimensions (Bejan, 1997b). Experimentally, the question is then one of how tall, or thick, these trees should be in order for a measurable cooling performance effect to be seen. It was expected that a tree with a height of a few hundred nanometers may be less effective at dissipating heat from the system than a tree a few orders of magnitude taller due to material properties considerations on the micro scale (Chiang et al., 2005). Five fin heights were selected for fabrication ranging from approximately 100 nm to 2500 nm.

The final test section variant addresses the issue of how to embed the tree into the substrate, and the best method for accomplishing this. Experimentally, this will help to

determine whether increasing the surface area of the constructal tree in contact with the heat generating volume will further enhance the cooling performance of the system.

1.5 Report Outline

Chapter 1 provided a context and motivation for this study. Also discussed were relevant work and literature, as well as what this study contributes to work in this area. The remaining chapters of this report will outline the project at different stages. Chapter 2 is concerned with explaining the design considerations and the fabrication of the test sections, and the methods used for accomplishing this task. Chapter 3 will outline the design of the experiment and the methodology devised for measuring the cooling performance of each test section. Chapter 4 of this report expresses conclusions and recommendations regarding the micro-fabrication techniques for creating test sections, and the experimental methodology.

Chapter 2 Test Section Fabrication Methods

2.1 Types of Test Sections

This chapter will discuss the design and fabrication methods used for creating the test sections. There were multiple types of test sections created for this experiment. The overall design can be split into two main categories that include unconstrained surface area trees, where the surface area of each constructal tree increases as the geometric complexity of the constructal tree increases, and constrained surface area trees. After determining whether the surface area is unconstrained or constrained, the next step is to select whether the tree is exposed, meaning deposited directly on the surface of the substrate, or embedded into the substrate. The final level corresponds to the selection of the substrate material, either glass or silicon. This selection process followed in this study is categorized by the flow chart in Figure 2-1.

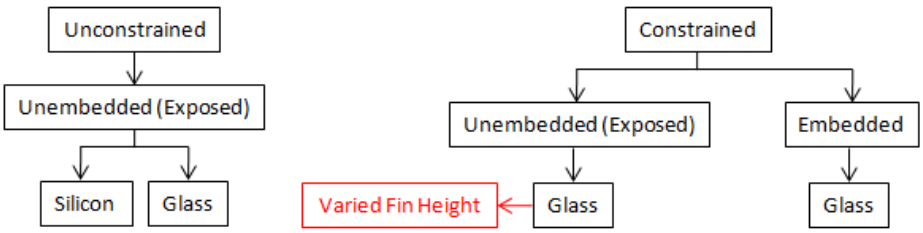

Figure 2-1: Flow chart showing the categories and variants of each set of test sections.

The red box in Figure 2-1 denotes that the height of the tree was varied during fabrication for that type of test section.

2.2 Test Section Geometry and Dimensions

A total of five constructal tree complexities were designed for testing, each with one more bifurcation than the preceding complexity starting with a zeroth order

complexity. Figures 2-2a through 2-2e illustrate the tree geometries and show a top view of the test sections. The white square area represents the substrate, and black rectangular networks represent the constructal trees.

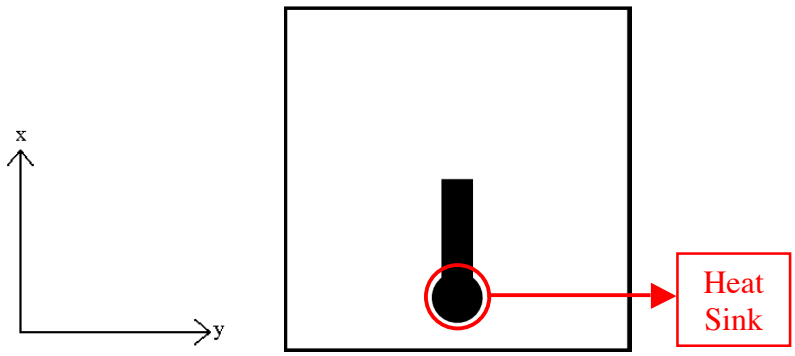

Figure 2-2a: Top view design of the zeroth test section complexity.

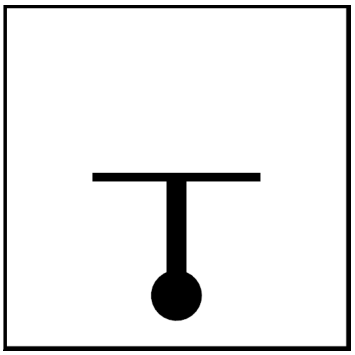

Figure 2-2b: Top view design of the first test section complexity.

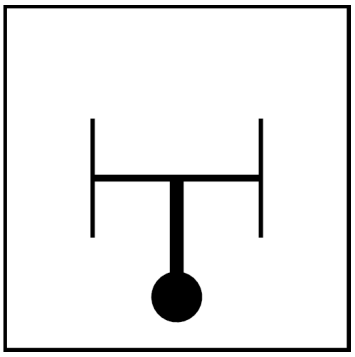

Figure 2-2c: Top view design of the second test section complexity.

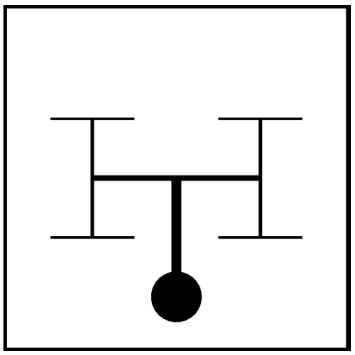

Figure 2-2d: Top view design of the third test section complexity.

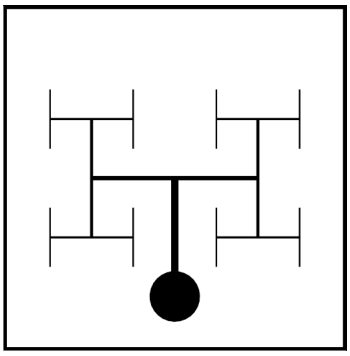

Figure 2-2e: Top view design of the fourth test section complexity.

The dimensions of the substrate were 1cm x 1cm. The largest tree branch is centered on the substrate, and the top edge is located at the midway point of the substrate, as shown in Figures 2-2a through 2-2e. The constructal tree branch dimensions follow the constraints listed in Equations 2-1 and 2-2 that govern the length and width relationships of each of the branches within each tree, and a methodology for setting the tree branch dimensions was recommended by literature (Murray, 1926; Bejan, 1997b; West and Brown, 1997; Bejan, 2000).

$$\frac{L_i}{L_{i+1}} = 2^{1/2} \qquad \text{(Eq. 2-1)}$$

$$\frac{W_i^h}{W_{i+1}^h} = 2^{1/3} \qquad \text{(Eq. 2-2)}$$

Where L_i is the length of the i^{th} constructal branch and L_{i+1} is the succeeding constructal branch, and W_i^h is the width of the i^{th} constructal branch (Murray, 1926; Bejan, 1997b; West and Brown, 1997; Bejan, 2000). The branch constraints dictated by Equations 2-1 and 2-2 were used in setting the dimensions for the constrained area constructal trees. For the unconstrained trees, the constraint suggested by Equation 2-2 (Murray, 1926; Bejan, 1997b; West and Brown, 1997; Bejan, 2000) was relaxed. The tree heights were constant for all five tree complexities in each set of test sections. The final additional design feature to each test section was the addition of the 1.5 mm diameter heat sink in the shape of the enlarged circular area at the tip of the constructal tree. This was a necessary design feature for the experiment and will be discussed later.

Tables 2-1 through 2-7 display the measured dimensions of each constructal tree for the different types of fabricated test sections. The actual length dimensions shown in these tables were similar to the ones used by literature (Hart and da Silva, 2010). Tables 2-1 and 2-2 show the measured dimensions of each tree branch for all five tree

complexities in each set of test sections for unconstrained trees with constant tree heights. Tables 2-3 through 2-7 show the measured dimensions for the constrained trees. With respect to the dimensions listed in Tables 2-3 through 2-7, it is important to note that in selecting these tree dimensions, the tree heights were again constant for all trees in each set. The lengths of each branch, i.e. $L_{K,0}$, $L_{K,1}$, etc. were constant between tree complexities and respect the relationship shown in Equation 2-1. With these length and height constraints in place, the widths of each tree branch, i.e. $W_{K,0}$, $W_{K,1}$, etc. were varied from tree complexity to tree complexity to create the constrained tree dimensions. Tables 2-3 and 2-4 list dimensions for all five complexities for constrained tree test sections having constant tree heights. Tables 2-5 through 2-7 list the dimensions for a single complexity with varied tree heights. In Tables 2-5 through 2-7 each of the tree branch width measurements may vary only slightly for each tree height listed due to fabrication tolerances achieved. The length, width and height measurements of each copper branch were taken using a Veeco model profilometer, which has a resolution in the angstrom length scale. Taking multiple measurements across each tree branch helped verify that every branch was uniformly the same height.

Table 2-1: Measured dimensions of constructal tree branches, $L_{k,n}/W_{k,n}$ (mm/mm), for unconstrained volume exposed fin on glass substrate test sections (H = 0.90 microns).

Complexity	$L_{K,0}/W_{K,0}$	$L_{K,1}/W_{K,1}$	$L_{K,2}/W_{K,2}$	$L_{K,3}/W_{K,3}$	$L_{K,4}/W_{K,4}$
0	3.500/0.3862	--	--	--	--
1	3.500/0.2734	2.475/0.1576	--	--	--
2	3.500/0.2383	2.475/0.1422	1.750/0.0945	--	--
3	3.500/0.2222	2.475/0.1355	1.750/0.0906	1.237/0.0634	--
4	3.500/0.2157	2.475/0.1315	1.750/0.0882	1.237/0.0626	0.875/0.0460

Table 2-2: Measured dimensions of constructal tree branches, $L_{k,n}/W_{k,n}$ (mm/mm), for unconstrained volume exposed fin on silicon substrate test sections (H = 1.20 microns).

Complexity	$L_{K,0}/W_{K,0}$	$L_{K,1}/W_{K,1}$	$L_{K,2}/W_{K,2}$	$L_{K,3}/W_{K,3}$	$L_{K,4}/W_{K,4}$
0	3.500/0.3856	--	--	--	--
1	3.500/0.2736	2.475/0.1573	--	--	--
2	3.500/0.2382	2.475/0.1425	1.750/0.0941	--	--
3	3.500/0.2223	2.475/0.1354	1.750/0.0902	1.237/0.0636	--
4	3.500/0.2152	2.475/0.1309	1.750/0.0887	1.237/0.0626	0.875/0.0450

Table 2-3: Measured dimensions of constructal tree branches, $L_{k,n}/W_{k,n}$ (mm/mm), for constrained volume exposed fin on glass substrate test sections (H = 2.52 microns).

Complexity	$L_{K,0}/W_{K,0}$	$L_{K,1}/W_{K,1}$	$L_{K,2}/W_{K,2}$	$L_{K,3}/W_{K,3}$	$L_{K,4}/W_{K,4}$
0	3.500/0.9232	--	--	--	--
1	3.500/0.5829	2.475/0.2554	--	--	--
2	3.500/0.4014	2.475/0.2039	1.750/0.1258	--	--
3	3.500/0.2896	2.475/0.1626	1.750/0.1054	1.237/0.0734	--
4	3.500/0.2157	2.475/0.1319	1.750/0.0886	1.237/0.0623	0.875/0.0448

Table 2-4: Measured dimensions of constructal tree branches, $L_{k,n}/W_{k,n}$ (mm/mm), for constrained volume embedded fin on glass substrate test sections (H = 2.76 microns).

Complexity	$L_{K,0}/W_{K,0}$	$L_{K,1}/W_{K,1}$	$L_{K,2}/W_{K,2}$	$L_{K,3}/W_{K,3}$	$L_{K,4}/W_{K,4}$
0	3.500/0.9222	--	--	--	--
1	3.500/0.5825	2.475/0.2551	--	--	--
2	3.500/0.4008	2.475/0.2034	1.750/0.1264	--	--
3	3.500/0.2893	2.475/0.1634	1.750/0.1052	1.237/0.0730	--
4	3.500/0.2153	2.475/0.1314	1.750/0.0884	1.237/0.0625	0.875/0.0450

Table 2-5: Measured dimensions of constructal tree branches, $L_{k,n}/W_{k,n}$ (mm/mm), for constrained volume exposed fin on glass substrate test sections (varied fin heights).

Fin Height (Microns)	$L_{K,0}/W_{K,0}$	$L_{K,1}/W_{K,1}$	$L_{K,2}/W_{K,2}$	$L_{K,3}/W_{K,3}$	$L_{K,4}/W_{K,4}$
0.116	3.500/0.9254	--	--	--	--
0.208	3.500/0.9248	--	--	--	--
0.521	3.500/0.9233	--	--	--	--
1.091	3.500/0.9227	--	--	--	--
2.520	3.500/0.9232	--	--	--	--

Table 2-6: Measured dimensions of constructal tree branches, $L_{k,n}/W_{k,n}$ (mm/mm), for constrained volume exposed fin on glass substrate test sections (varied fin heights).

Fin Height (Microns)	$L_{K,0}/W_{K,0}$	$L_{K,1}/W_{K,1}$	$L_{K,2}/W_{K,2}$	$L_{K,3}/W_{K,3}$	$L_{K,4}/W_{K,4}$
0.116	3.500/0.4016	2.475/0.2045	1.750/0.1265	--	--
0.208	3.500/0.4006	2.475/0.2037	1.750/0.1258	--	--
0.521	3.500/0.4010	2.475/0.2034	1.750/0.1258	--	--
1.091	3.500/0.4008	2.475/0.2042	1.750/0.1262	--	--
2.520	3.500/0.4014	2.475/0.2039	1.750/0.1258	--	--

Table 2-7: Measured dimensions of constructal tree branches, $L_{k,n}/W_{k,n}$ (mm/mm), for constrained volume exposed fin on glass substrate test sections (varied fin heights).

Fin Height (Microns)	$L_{K,0}/W_{K,0}$	$L_{K,1}/W_{K,1}$	$L_{K,2}/W_{K,2}$	$L_{K,3}/W_{K,3}$	$L_{K,4}/W_{K,4}$
0.116	3.500/0.2154	2.475/0.1308	1.750/0.0883	1.237/0.0618	0.875/0.0446
0.208	3.500/0.2157	2.475/0.1310	1.750/0.0880	1.237/0.0620	0.875/0.0446
0.521	3.500/0.2158	2.475/0.1314	1.750/0.0886	1.237/0.0624	0.875/0.0450
1.091	3.500/0.2156	2.475/0.1316	1.750/0.0888	1.237/0.0626	0.875/0.0454
2.520	3.500/0.2157	2.475/0.1319	1.750/0.0886	1.237/0.0623	0.875/0.0448

2.3 Fabrication Methods

After the design phase, the next step was fabrication. Several processes and stages were required to make suitable test sections. These stages included photolithography, reactive ion etching, thin metal deposition, cutting and sectioning with a dicing saw, and application of PDMS. The step order is shown in a flow chart in Figure 2-3.

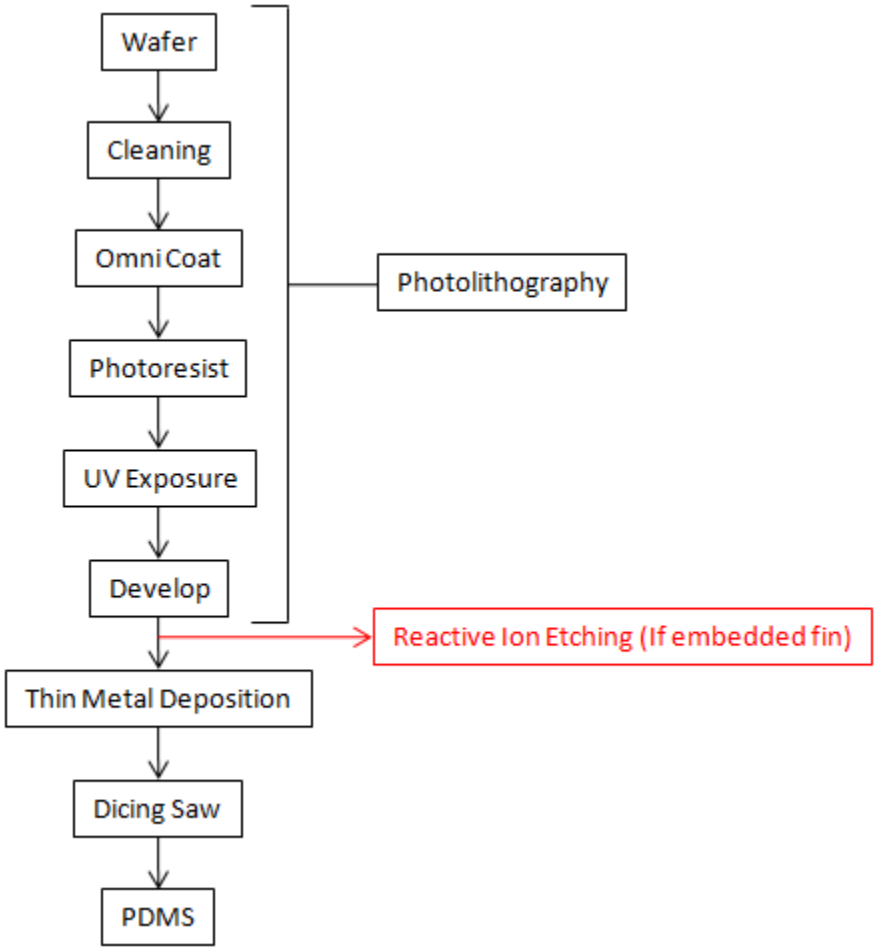

Figure 2-3: Process flow chart showing the test section fabrication steps.

The red box in Figure 2-3 indicates that an extra etching step was necessary for embedded trees. The remainder of this chapter will outline each of these techniques and the need for them in the fabrication process.

2.3.1 Photolithography

The first step was to determine a way to deposit the copper trees uniformly, and to produce the dimensions discussed in section 2.2. Based on available metal deposition techniques, the best way found to accomplish this was to create a "mold" in which to deposit the copper. An easily moldable thermosetting polymer, referred to as photoresist, was found to be ideal for creating the molds (Lorenz et al., 1997; Zhang et al., 2001). Photoresist is initially in liquid form and is available in different consistencies, viscosities, and chemistries. After applying to a substrate and following various baking and curing processes, the photoresist is exposed to high energy density UV radiation that cures it and makes it solid and adhered to the surface. After the UV exposure, a final developing step is needed to etch the "molds" using a wet acetate based solution, or a dry plasma clean (Lorenz et al., 1997). Ideally, this process will yield high wall molded channels that can be filled with copper. The final product of an exposed and developed photoresist mold is shown in Figure 2-4.

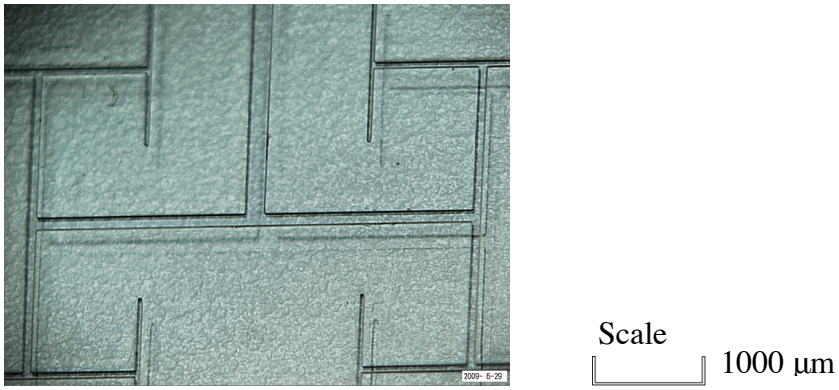

Figure 2-4: Developed photoresist mold on a glass substrate (100x magnification).

A lithography mask was needed for the UV exposure step. A sample rendering of the lithography mask used is shown in Figure 2-5. The photoresist used had a negative polarity, therefore the blackened areas resembling the constructal trees in Figure 2-5 were necessary to ensure those areas were etched and removed during development (Lorenz et al., 1997). Each constructal tree was drawn using Solidworks modeling software, and rendered into a 2-D drawing to make the lithography mask. The dimensions of each constructal tree conform to the constraints discussed in section 2.2. The final product was printed using a high resolution printer on a transparent sheet.

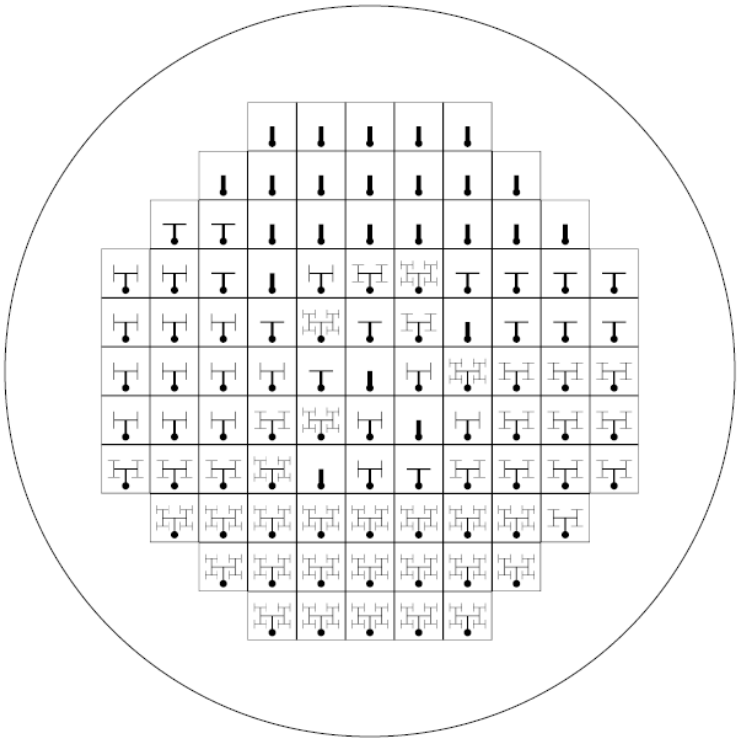

Figure 2-5: Design of the photolithography mask used (diameter: 6-inches).

The wafers used for the unconstrained tree test sections were 6-inch diameter silicon wafers with a thickness of 560 microns, and 6-inch diameter borosilicate glass wafers with a thickness of 700 microns. The wafers used for the constrained tree test sections were 4-inch diameter borosilicate glass wafers with a thickness of 200 microns. The photoresist used was SU 8-2075 for its high viscosity and ability to create thick layers with a single coat (Microchem: SU 8-2000, 2009). One issue with SU 8-2075 is that it is not easily removed from a substrate once fully cured after UV exposure (Dettinger et al., 2002). Therefore, it was necessary to use a "release" layer under the photoresist, one which could be chemically dissolved and would facilitate the removal of the SU 8-2075 layer after depositing the copper trees (Song and Ajmera, 2003). The release layer used was Omni coat because it can be cured onto the surface of a substrate without affecting the photoresist during the fabrication process, and is easily dissolved using acetone (Microchem Corp: Omni Coat, 2009).

The first step in the photolithography process was proper substrate preparation and cleaning. The removal of oxides, oils and organic residue was necessary to ensure proper adhesion of the photoresist throughout further processing steps (Microchem: SU 8-2000, 2009). The substrates were wet cleaned and rinsed with acetone, isopropyl alcohol, distilled water, and dried using nitrogen gas. After wet cleaning, dry cleaning was done using a plasma clean process to further remove residuals and organics. Plasma cleaning uses the process of reactive ion etching to scavenge organics and remove residuals (Rossnagel et al., 1990). An O_2 gas with a flow rate of 30 SCCM, a power of 100 Watts and a time of 120 seconds was used to remove residuals and organics (BYU, 2009). Following this cycle, a gas combination of 10 SCCM of SF_6 and 30 SCCM of O_2, a power of 100 Watts and a time of 100 seconds was used to remove the initial atomic layers of the substrate (Rossnagel et al., 1990).

After substrate cleaning, a layer of Omni coat was applied to the surface of the substrate. Instructions for properly applying and curing the Omni coat were provided by the manufacturer, Microchem, and followed throughout the fabrication process (Microchem Corp: Omni Coat, 2009). The next step was to apply the photoresist layer. Instructions for proper application of the photoresist, SU 8-2075, were provided from the manufacturer, Microchem, and followed throughout the fabrication process (Microchem: SU 8-2000, 2009). Processing steps included application, spin coat, soft bake, exposure, hard bake, and development (Microchem: SU 8-2000, 2009).

During the exposure step, the sample was exposed to filtered UV light with a radiation intensity of nominally 10 W/cm^2. The radiation was filtered using an I-line filter in order to prevent light with wavelengths less than 300 nm from passing through to the sample. This helped to ensure that straight-walled channels would be produced in the overall sample (Williams and Wang, 2004). After exposure, the sample was developed by submersing in an acetate based development solution called SU 8 Developer. In early fabrication attempts, residual photoresist remained in the channel after the recommended development time was reached. This residual resist that remained in the channels is seen with a microscope and shown in Figure 2-6, and can be compared to Figure 2-4 which has no residual resist. The residual photoresist left over was removed using a dry etch, or reactive ion etching process with O_2 gas at 35 SCCM gas flow rate, a power of 100 Watts and a time of 60 seconds (Microchem Corp: SU-8 2000, 2009). A photoresist thickness of approximately 70 microns was produced from this process, a thickness verified by measuring with a Veeco model profilometer.

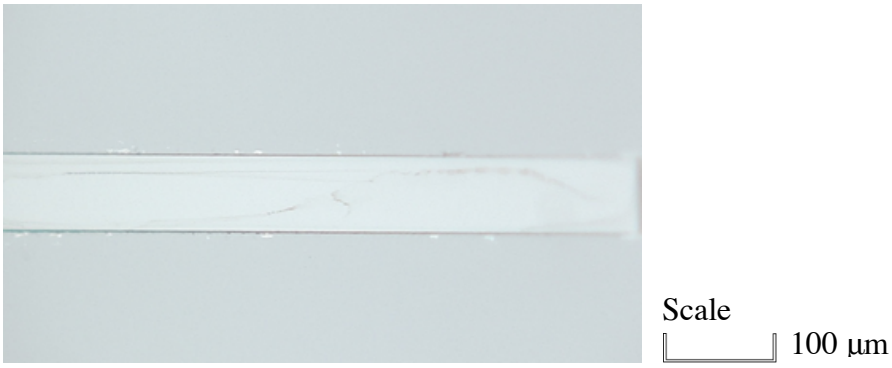

Figure 2-6: Microscope photo showing residual photoresist within the assembly channel of a silicon sample (150x magnification).

2.3.2 Reactive Ion Etching

The embedded tree samples were created using a reactive ion etch step following photolithography. The concept behind reactive ion etching is the use of a reactive gas to remove surface residuals or even atomic layers from a substrate (Rossnagel et al., 1990). This is accomplished by ionizing the molecules of the reactive gas with a resonating electromagnetic field, after which the gas molecules anisotropically collide with the surface to react with and remove the residuals or surface atomic layers. Depending on the power input and flow rate of the gas into the chamber, the etch rate of the substrate can be regulated (Rossnagel et al., 1990).

The embedded samples had glass substrates. Several steps were needed within a single gas recipe, including a chamber oxide removal step, gas deposition of C_4H_8, and finally the etch cycles using a recommended gas mixture for glass etching (Zhou, 2009). Initially the sample was placed into a chamber and which was then evacuated. A deoxidizing step was initially performed to facilitate etching, followed by an initial deposition of a C_4H_8 layer covering the sidewalls of the photoresist channels. This was to prevent inward etching of the photoresist to ensure straight wall resist molds were

maintained. After this deposition, the etching process was initiated using a gas chemistry recommended for etching silicon dioxide (Zhou, 2009). Table 2-8 includes the gas chemistries and flow rates.

Table 2-8: Gas chemistry and flow rates used for etching silicon dioxide.

Reactive Gas	Approximate Flow Rate (SCCM)
N_2	2
O_2	1
SF_6	100
CF_4	30

The etch rate of the glass using this gas combination was approximately 70 nanometers per cycle. Approximately 40 gas etch cycles were run to produce a final etch depth of 2.76 microns. The etch depth of the process was verified by measurements using a Veeco model profilometer.

2.3.3 Thin Metal Deposition of the Constructal Trees

Two methods were studied and evaluated for depositing the copper trees including thermal evaporation deposition and copper sulfate electroplating. The limitations and advantages of each process were considered, and will be discussed in the following.

2.3.3.1 Electroplating

Electroplating is a method capable of "growing" very thin layers of a metal like copper onto a surface. Typical deposition thicknesses fall within the range of a few dozen microns to a few hundred microns in thickness (Andricacos et al., 1998; ASM: Plating, 2002). This relatively old concept requires an electric circuit to attract charged copper

atoms onto a conducting surface. In the case of copper sulfate electroplating, the sample to be plated is connected to a negative terminal, called the cathode, and a piece of high purity copper, usually a solid copper bar, is connected to the positive terminal, called the anode. The cathode and anode are placed within a copper sulfate bath and a current is applied, which ionizes the copper sulfate salt and produces positively charged copper atoms. The current causes the cathode to become negatively charged, attracting the positively charged copper atoms. The end result is the deposition of copper onto the cathode (ASM: Plating, 2002).

In order for the deposition to occur, the sample must have a conductive layer to facilitate the electrically driven deposition process. This conductive layer is referred to as a "strike" layer and must be sufficiently thick, usually greater than 100 nm, which can be deposited on the substrate via thermal evaporation (Andricacos et al., 1998). The bath chemistry used consisted of a mixture of 4 parts distilled water, and 1 part copper sulfate pentahydrate, $CuSu_4 5H_2O$ (ASM: Plating, 2002). Proper preparation of the sample surface for deposition was required. This consisted of plasma cleaning the cathode with O_2 at a flow rate of 35 SCCM and a power of 100 Watts for 30 seconds (Rossnagel et al., 1990). Anode cleaning was also critical in minimizing bath contamination. ASTM procedures for the cleaning of the copper anode in preparation for electroplating were followed (ASTM 281, 2002). The current density recommended for creating small-grained copper deposits is on the order of 0.01 Amps/cm^2 (ASM: Plating, 2002). A 60 Watt Omega PSU304 power supply with 1.0 Amp current capacity and +/- 30 Volt voltage capacities supplied the current; however, the lowest attainable current density was 0.05 Amps/cm^2.

In running the electroplating process in its entirety, it was found that the process was inconsistent and difficult to control. As a result of this limitation, large grains of copper were deposited onto the substrate surface. Since the grains were large, it was

possible that they were not in good contact with one another, and the overall effective thermal conductivity of this constructal tree was thought to be far below that of the bulk properties of copper (Dubin et al., 1997). A microscope picture illustrating the large grains and the surface roughness is shown in Figure 2-7.

Figure 2-7: Microscope picture of copper deposited by means of electroplating process (50x magnification).

It was found through fabrication attempts that due to the issues associated with the quality of the deposited copper trees, as well as repeatability and controllability issues in the process itself, electroplating was not a suitable method for the deposition of the constructal trees. Therefore other more suitable and reliable methods such as thermal evaporation were explored for completing the deposition process.

2.3.3.2 Thermal Evaporation Deposition

Thermal evaporation is a process where a metal like copper is melted down in a vacuum chamber and condensed onto a surface (ASM: Vacuum coating, 2002). The

advantages of this method are that highly uniform deposition of metals is possible. It is also possible to meet very small dimensional tolerances on the order of the nanoscale (Kurt J. Lesker Company, 2009). Furthermore, because of how the deposition occurs, the electrical and thermal properties of the deposited metal are often very close to that of the bulk properties of the metal (ASM: Vacuum coating, 2002). The disadvantages of this technique are that very low deposition rates are necessary for completing the process. The maximum attainable layer thicknesses obtained are often approximately 0.5-3.0 microns for one deposition cycle (ASM: Vacuum coating, 2002).

The thermal evaporation process requires a high current low voltage source to melt the metal, and a vacuum chamber to minimize surface oxidation and lower the chamber pressure during deposition. A sample is properly cleaned, usually with an O_2 plasma clean, to improve adhesion of the metal layer to the surface (Rossnagel et al., 1990). In this case, the cleaned substrate was placed into the thermal evaporator along with the copper metal, and the chamber was pumped to a pressure of 10^{-5} Torr. A deposition rate of approximately 0.5-1.2 Angstroms/second was maintained. A quartz-crystal monitor was used to measure the instantaneous deposition rate and deposition thickness of the copper layer. The quality of the deposited layer using thermal evaporation was much higher than that of the layer produced using electroplating. The quality and continuity of the deposited trees via thermal evaporation can be shown in Figures 2-8 and 2-9, and compared to the electroplated tree in Figure 2-7.

The overall tree thicknesses achieved ranged from approximately 1 micron for the unconstrained trees, up to nearly 3 microns for the constrained trees. This was measured and verified using a Veeco profilometer. Figure 2-9 shows the smallest test section feature, which is a branch 46 microns in width and 0.9 microns in height. Also notice the sharp right angles achieved by this deposition process.

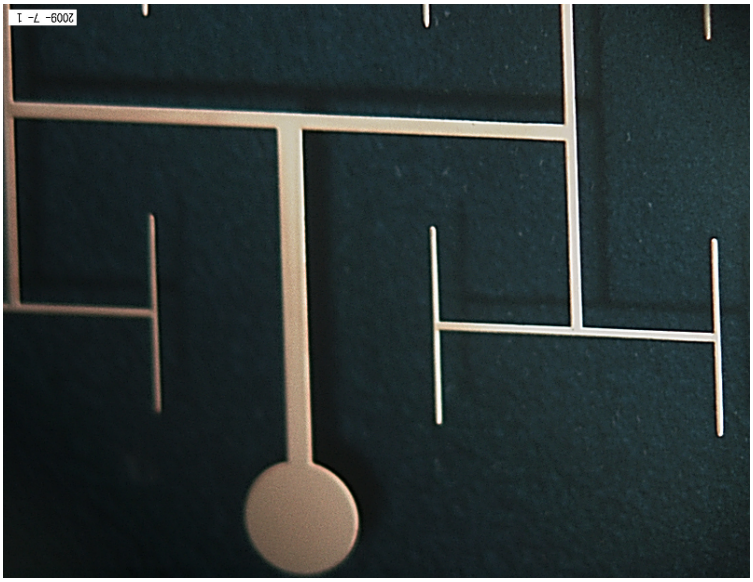

Figure 2-8: Microscope photo of test section geometric complexity 4 illustrating the uniformity of the deposited copper layer (50x magnification).

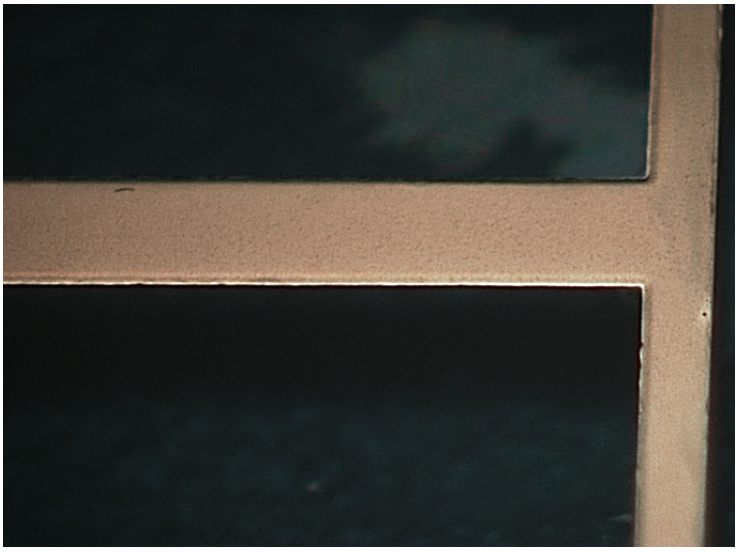

Figure 2-9: Microscope photo of test section close-up illustrating the uniformity, the thickness and tolerance of the deposited copper layer (350x magnification).

2.3.4 Finalizing the Test Sections

This process began with sectioning the wafer into 1cm x 1cm squares. An effective and accurate tool for sectioning the wafer into these squares was a dicing saw. This is a device that allows a high-precision automated program to run in order to make multiple cuts spaced a particular distance apart. A wafer can be "diced" into rectangular or square shapes depending on the cut dimensions set in either the longitudinal or lateral directions of the wafer (Boucher and Bajune, 1997). Once the sample was sectioned appropriately to the desired dimensions, the next step was to remove the photoresist mold from the test section. This was done by soaking each of the test sections in an acetone bath with heat and agitation from an ultra-sonic bath for a period of approximately 30 minutes (Microchem Corp: Omni Coat, 2009). A sectioned test section with the photoresist removed is shown in Figure 2-10. Notice that according to the ruler measurement, the sample was accurately sized to the appropriate 1cm x 1cm dimension, illustrating the effectiveness of the dicing saw for the sectioning process.

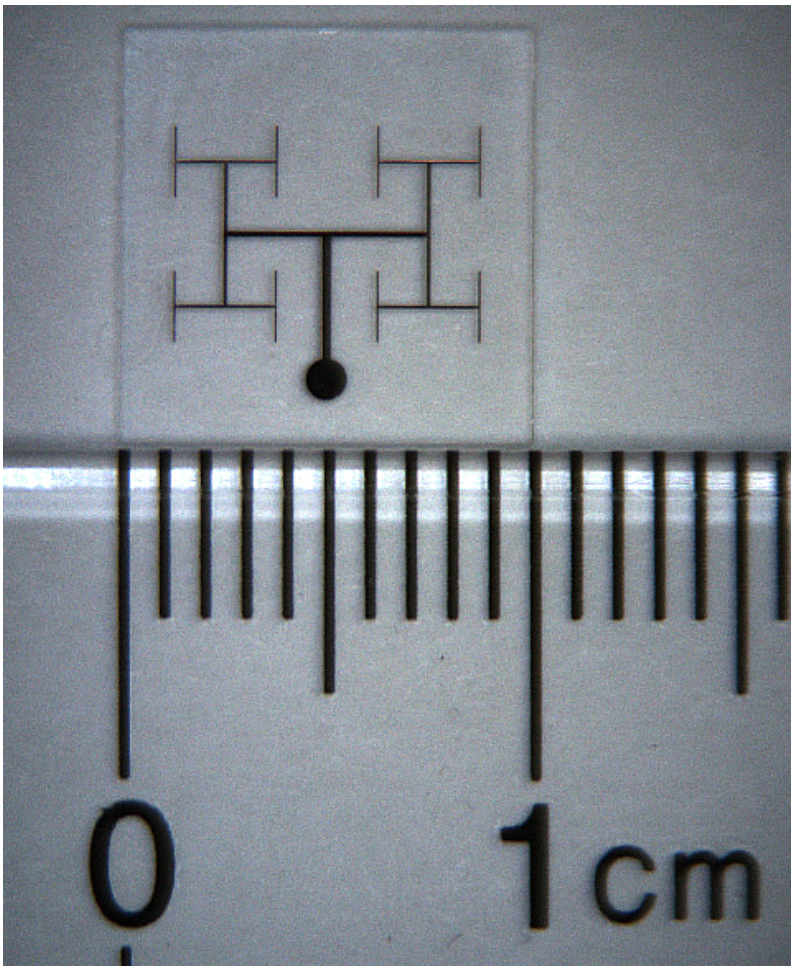

Figure 2-10: Microscope photo illustrating the size scale of a test section.

In order to provide another perspective of size and scale, a photo of a test section next to a penny is shown in Figure 2-11. The very small scale of this system should become very evident in this figure.

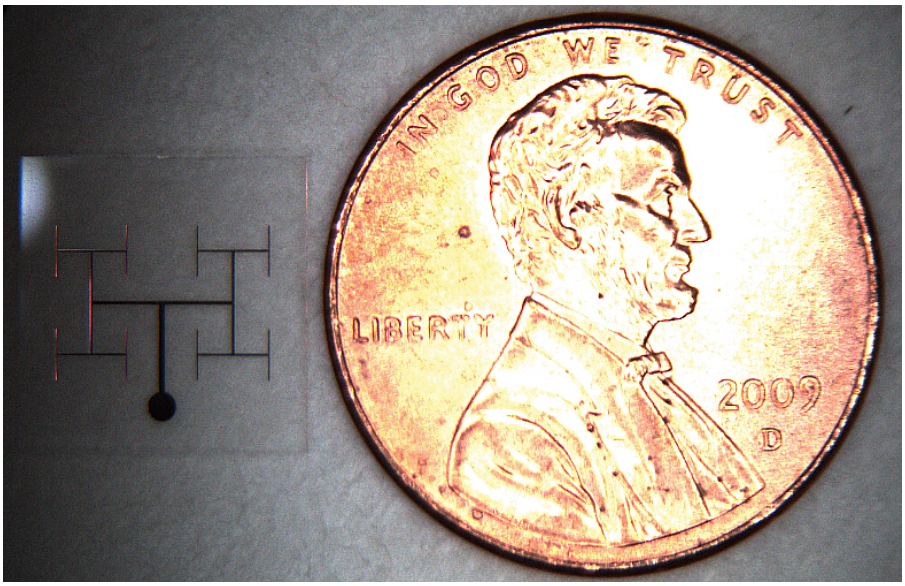

Figure 2-11: Microscope photo illustrating the size scale of a test section in comparison to the size of a penny.

2.3.4.1 Application of PDMS

For this experiment the conduction heat transfer performance of the system is the focus. Therefore removing any outside convection affects from the surroundings is desired. This was accomplished by insulating the constructal tree and substrate surface with a thick, low thermal conductivity material. Polydimethyl siloxane, or PDMS, was used because it has a very low thermal conductivity making it a good insulator, and it is easy to mold (Papra et al., 2001; Chang-Yen et al., 2005; MIT, 2010). This allows for the heat sink area to be easily exposed, a necessary aspect of the experiment that will be explained later.

A small jig was built to facilitate the shaping of the PDMS onto and around each of the test sections. Photos of the jig used are shown in Figures 2-12 and 2-13. The jig was built to accommodate up to five test sections, to include every tree complexity, lined

up in a row to aid in producing constant insulation thicknesses for each test section. Since the PDMS is initially in liquid form, aluminum foil was used to prevent run-off and dripping, and to help in shaping. When placed on a flat surface, the liquid PDMS was allowed to cure over a period of 48 hours at standard conditions.

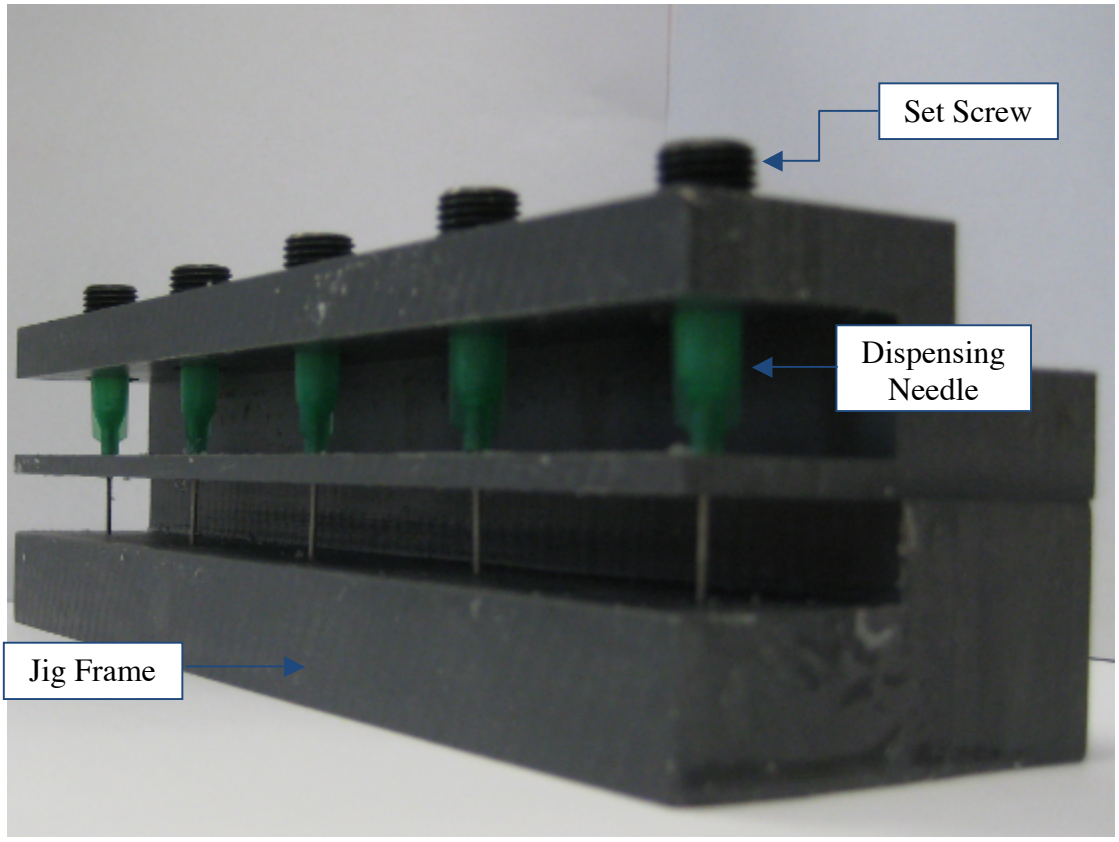

Figure 2-12: Perspective photo of the jig used to apply PDMS.

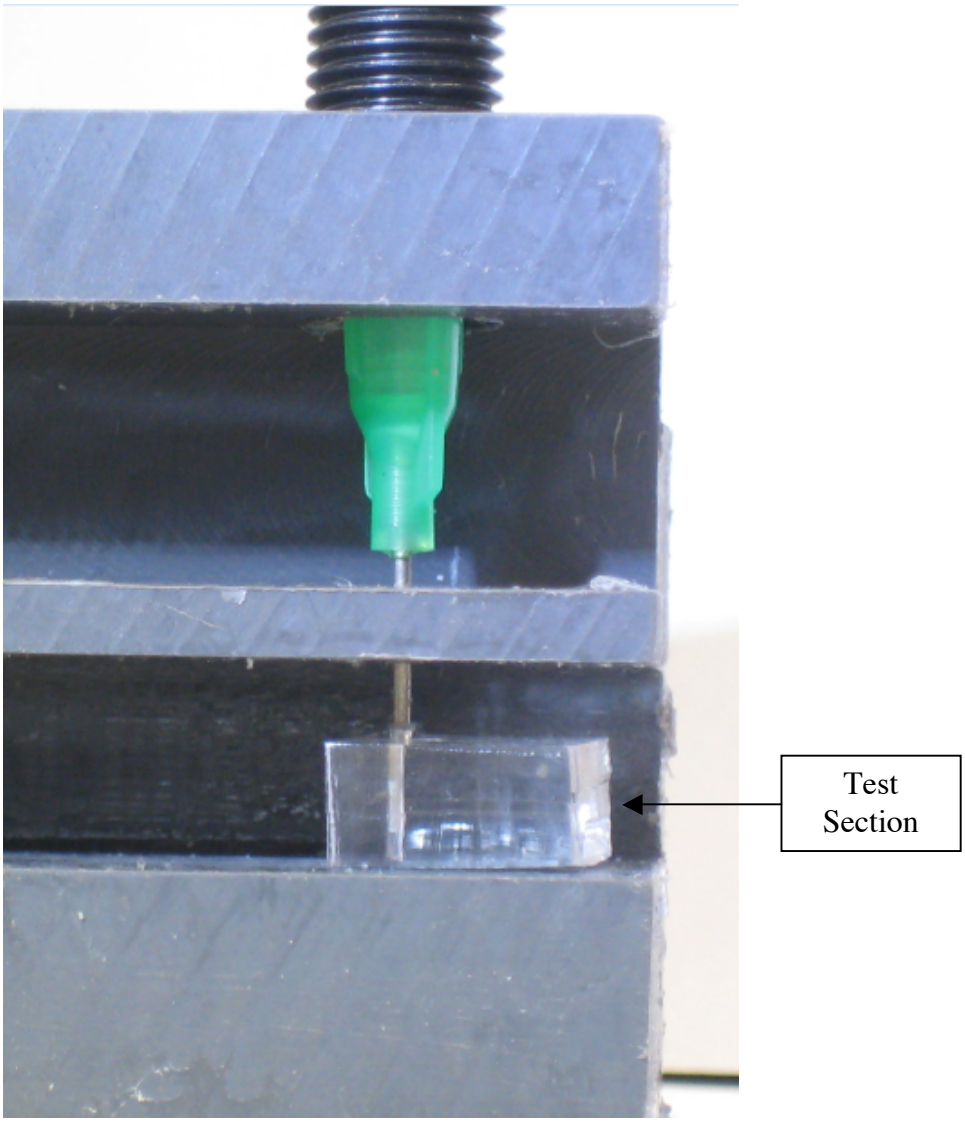

Figure 2-13: Front-view of jig slot including positioned test section.

A dispensing needle was used to shape the PDMS to expose the heat sink. The dispensing needle has a flat bottom, and an outer diameter approximate to that of the heat sink diameter (see Figure 2-2a). The dispensing needle tip was centered over the heat sink, and the needles were mounted vertically into the jig frame to ensure no slipping, good contact, and to prevent coating of the heat sink. A set screw was seated in the upper

part of the needle to aid in alignment, and to apply pressure on the needle against the heat sink. Cross-section schematics for both the finalized exposed and embedded fin type test sections are shown in Figures 2-14 and 2-15. Once fully cured, the needles were removed, exposing the heat sink. The excess PDMS was cut away from each of the test sections, and the final product was a test section containing a 1 cm x 1 cm substrate, and a 1 cm x 1 cm PDMS layer approximately 1/4" inch thick.

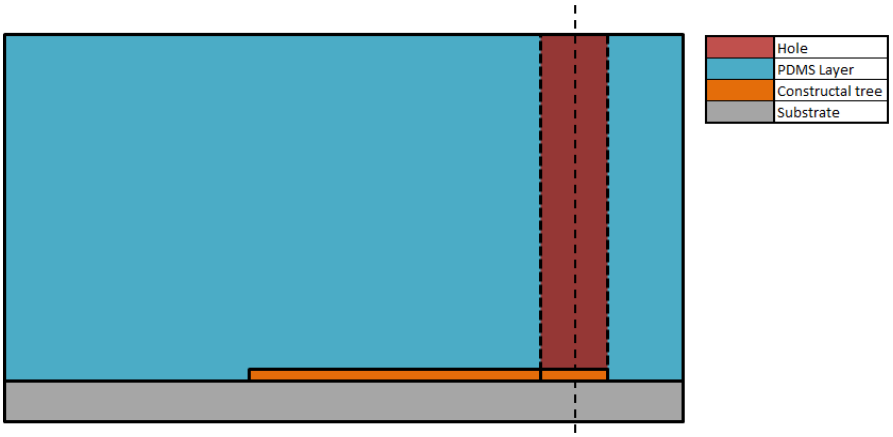

Figure 2-14: Schematic cross-sectional view of a finalized test section for exposed fin.

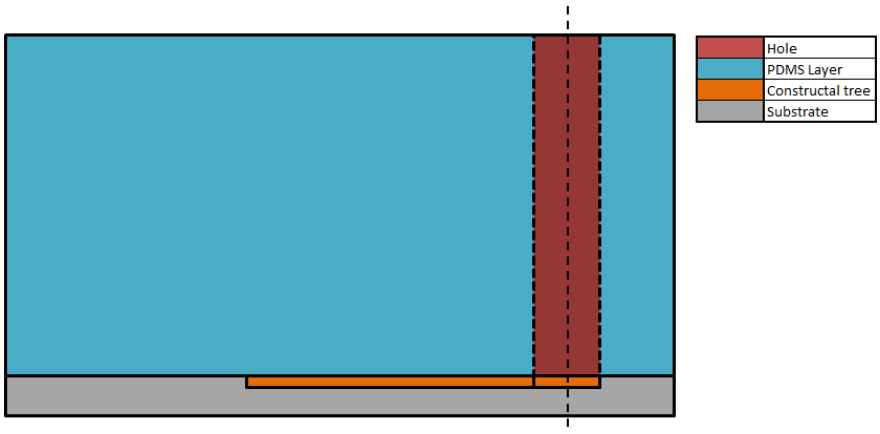

Figure 2-15: Schematic cross-sectional view of a finalized test section for embedded fin.

Chapter 3 Experimental Methodology

3.1 Experiment Setup and Equipment

This chapter will discuss the design of the experimental set-up, the equipment, and the methodology used for measuring the cooling performance of each test section. The experiment requires controlled heating to input heat to the test sections. A resistance heater with a controllable input, identical to the one designed by Hart and da Silva (Hart and da Silva, 2010), was built to accomplish this. A schematic cross-sectional diagram of the heater is shown in Figure 3-1. A machined copper block with cross-sectional dimensions of 1 cm x 1 cm, and a length of 10 cm, was used because of its high thermal conductivity, and consequently its ability to more uniformly distribute heat to the test section. The copper block was bored from the bottom and a resistive heating element was placed into the area, and the resistive element leads were connected to a 60 Watt Omega Engineering PSU304 power supply, and a constant DC voltage was supplied. Omega Engineering T-type thermocouples were attached to each side of the copper block to measure the surface temperature during the experiment (Hart and da Silva, 2010), and T-type thermocouples were selected since for the expected experimental operating temperatures, approximately 0-70 ˚C, the accuracy was the best available, to within +/- 0.5 ˚C (Omega: Thermocouples, 2009). After the thermocouples were attached, the entire unit was then centered inside a thin walled PVC tube with a 4 cm inner diameter, where the void between the unit and the tube wall was filled with a solidified layer of PDMS (Hart and da Silva, 2010). The outside of the PVC tube was insulated with a 1.5-inch thick layer of foam insulation. An insulating lid was also created to reduce convection and radiation heat losses to the surroundings.

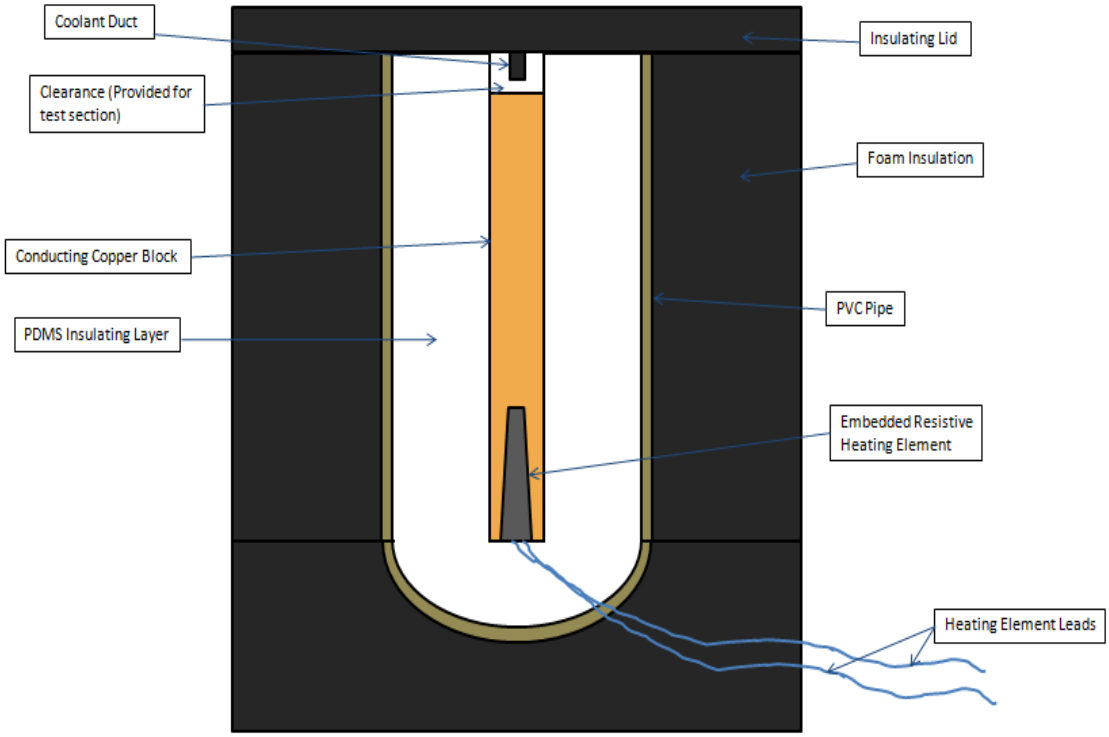

Figure 3-1: Schematic cross-sectional view of the heater and components used for the heat input to the test section.

The experiment also required a method for stimulating heat flow within the system by creating a heat sink: a test section design feature previously discussed in Chapter 2 of this report. A chilled fluid was impinged onto the surface of the heat sink in order to create the desired condition. In this experiment, the chilled fluid, or coolant, used was high purity nitrogen gas. An advantage to using nitrogen gas was that it would not wet itself to any surfaces and would simply exhaust to the atmosphere, which made handling the coolant fluid easier. A heat exchanger using copper tubing submersed in a low temperature bath was used to cool the nitrogen. An RTE 7 model chiller unit was used to regulate the bath temperature. This was ideal since the chiller bath temperature could be selected with a set point, and the chiller unit was designed to maintain the bath

temperature to within +/- 0.1 ˚C of the set point temperature (Thermo Scientific: RTE, 2009). This was important for ensuring that the inflow temperature of coolant gas was maintained constant. Thick layers of foam insulation were added to the tubing carrying the nitrogen from the chiller to minimize surrounding gains. The low temperature bath contained a 50/50 mixture of ethylene glycol and distilled water since the bath was operated at sub-zero temperatures (Thermo Scientific: RTE, 2009).

The insulating lid previously discussed was used to aid in handling the path of the coolant fluid as it entered and exited the heat sink area of the test section. A schematic diagram showing the lid and the intended coolant fluid path is shown in Figure 3-2. A nylon T-fitting (Figure 3-2) was used to accommodate three things: the inflow of the nitrogen gas from the chiller unit, a dispensing needle, and an Omega Engineering T-type thermocouple probe to measure the inflow coolant gas temperature (Omega: Thermocouples, 2009). A dispensing needle made of stainless steel with an outer diameter of 0.91 mm flowed the coolant into the heat sink area. This dispensing needle was also insulated with a thick layer of vinyl tape to minimize system gains, and to prevent any condensation from forming on the outside of the needle in the event that the coolant temperature was below the dew point temperature of the surrounding air (Callen, 1985). Since the dispensing needle was thin walled, during initial experiments without the vinyl tape, condensation was observed when the coolant temperatures were near 0 ˚C.

A final consideration included the following. Since the temperature of the nitrogen coolant gas was measured at a point in the T-fitting junction rather than at the very tip of the dispensing needle (Figure 3-2), there was possibility for coolant temperature gains. As a check, the temperature of the coolant gas was measured using the thermocouple in the T-fitting, and using a thermocouple placed at the tip of the dispensing needle. The difference in temperature was found to be less than 0.5 ˚C, which

is within the uncertainty or the accuracy of the thermocouple (Omega: Thermocouples, 2009).

A compatible data acquisition system was incorporated into the experiment to take measurements and log trends over time. This aided in determining when steady conditions were reached, and in assessing if any steady state variation between results occurred. The NI-DAQ system provides compatibility with LabVIEW, and allows an interface for all of the measuring equipment used in the experiment. This included temperature, coolant mass flow rate, and voltage and current readings from the power supply. A custom LabVIEW VI was created to help measure and log all of the data associated with the experiment. The data was tracked over time with a sampling rate of approximately 1 measurement every 1.8 seconds.

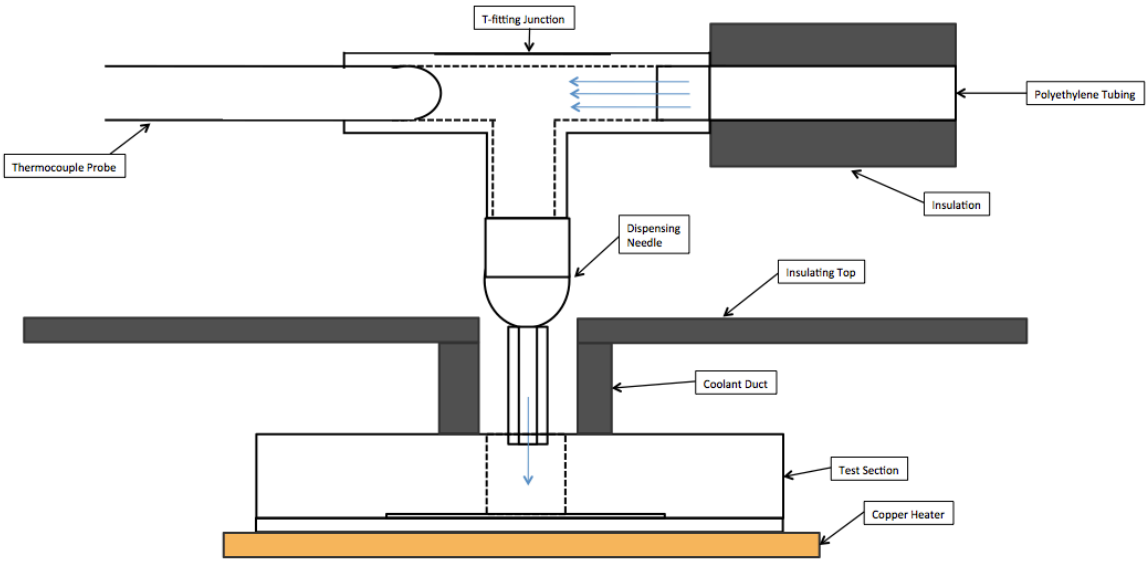

Figure 3-2: Schematic layout of coolant flow to heat sink path and inflow/outflow measurement apparatus.

3.2 Evaluation Criteria

The initial concept behind the experimental methodology was to supply a constant power input from the power supply to the heater, impinge the coolant nitrogen on the test section heat sink, and evaluate cooling performance based on measuring the test section substrate surface temperature at steady state conditions. For example, each test section was placed onto the heater apparatus separately, a constant heat input of 0.5 Watts, 1.0 Watts and 1.5 Watts would be supplied, and a constant stream of coolant fluid would impinge on the heat sink surface. The system would be allowed to operate under these conditions until steady system temperatures were reached, which was observed by monitoring the temperatures and determining when stability has been reached. It was hypothesized, based on theoretical studies (Bejan, 1997b; Bejan, 2000), that if progressively more complex trees produced proportionally lower surface temperatures under constant conditions, perhaps a correlation between tree complexity and cooling could be observed.

The first step was to place the test section onto the heater. An important consideration for improving the accuracy of the experiment was to reduce the contact resistance between the test section and the heater. The contact resistance would arise from inadequate pressure applied between surfaces, as well as from voids and pores on each surface. Therefore, to reduce these effects a thermally conductive paste was applied to the bottom of the test section surface, which was the surface in contact with the heater (Chung, 2001). Omega Engineering Thermal Paste was used for this application (Omega: Epoxies, 2009). Pressure was applied to the top of the test section via taught rubber bands to improve contact between surfaces and prevent any delaminating.

The ambient temperature was measured during each experimental trial and found to lie between 23 ˚C and 25 ˚C. The coolant temperature was set to be approximately 24 ˚C. During the experiment, two points on the surface of the substrate were measured with

Omega Engineering T-type hypodermic needle thermocouples, which punctured the PDMS and were placed in contact with the substrate surface. The points on the substrate that were measured are shown in Figure 3-3.

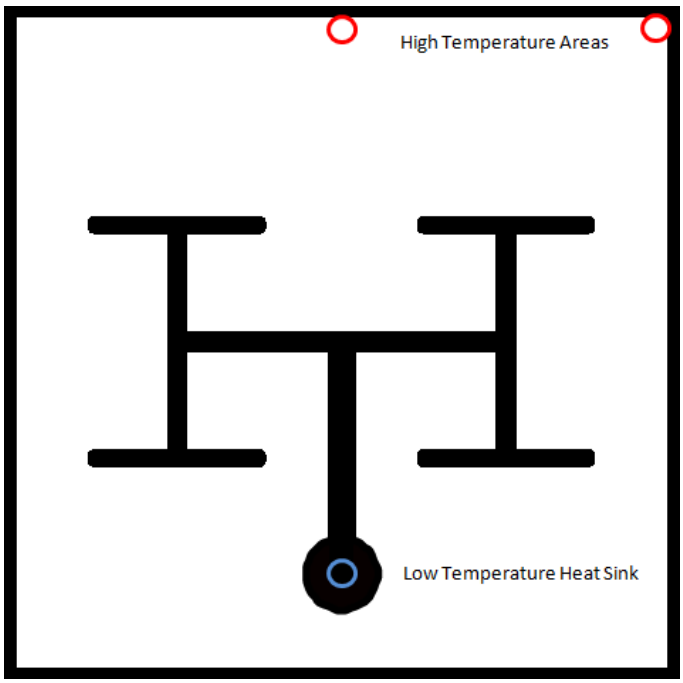

Figure 3-3: Diagram showing a top view of the test section, and showing areas where the temperatures were measured.

In running the experiment, the test section surface temperatures were found to vary from 7 ˚C lower than the heater temperature for a power input of 0.5 Watts, to up to a difference of 25 ˚C for a power input of 1.5 Watts. As a follow-up, the outside temperature of the foam insulation covering the heater was measured and found to be nearly 15 ˚C warmer than the surrounding temperature for a power input of 1.5 Watts. This temperature difference suggested that heat was being lost to the surroundings. It was difficult to determine exactly how much heat was being lost during each experimental

trial, and it was also thought that the accuracy of any measurements taken was being affected; these observations agreed with literature (Hart and da Silva, 2010). Therefore, the methodology for testing needed to be refined.

In order to minimize losses the present study relied on the methodology used by Hart and da Silva (Hart and da Silva, 2010), which realizes that it is desirable that the temperature of the system, including the temperature of the heater and substrate, be approximate to that of surrounding temperature. This would in fact become the most effective method for evaluating the test sections in this experiment. The system temperature would be held to the ambient temperature, and the coolant temperature would be cooled below the surrounding temperature to induce heat flow from the system to the heat sink. When the chilled nitrogen gas is impinged on the surface of the heat sink, it is removing a certain amount of heat from the system. Therefore, in order to ensure that the system was maintained at the surrounding temperature, a proportional amount of heat would need to be input into the system from the heater (Hart and da Silva, 2010).

A metric for quantifying heat losses during the experiment in the form of measuring the change in enthalpy of the coolant gas and comparing it to the heater input from the power supply was used (Hart and da Silva, 2010). It was thought that if the overall percent change between the change in enthalpy and the heat supplied by the power supply was on the order of a few percent, then it was safe to assume that for the experiment, heat losses were small. The change in enthalpy of the coolant gas was measured using the following formula given in Equation 3-1 (Incropera et al., 2006).

$$\dot{Q} = \dot{m} c_p (T_{out} - T_{in}) \qquad \text{(Eq. 3-1)}$$

Where $\dot{Q}$ is the change in enthalpy, ṁ is the gas mass flow rate, c_p is the specific heat of nitrogen, T_{out} is the outflow temperature of nitrogen and T_{in} is the inflow temperature of nitrogen (Incropera et al., 2006).

A dual stage regulator was used to aid in providing a steady flow of nitrogen gas to the system. During the experimental trials, an Omega Engineering digital flow meter was used to measure the coolant gas mass flow rate. This device provided a direct measure of mass flow rate, as well as an overall increased measurement accuracy. The specific heat, c_p, of the nitrogen was assumed to be constant and unchanged during the experiment. This is due to that fact that in the range of temperatures experienced in the nitrogen between the inflow and outflow stages, there is a negligible change in specific heat (Incropera et al., 2006; NIST, 2009).

3.3 Experimental Settings and Test Results

The described experimental methodology was tested, and data points were obtained in order to validate this methodology. A constrained surface area tree test section with a tree height of 2.52 microns and a zeroth order tree complexity (Figure 2-2a) was tested. After an initial test, in order to verify the precision and repeatability of the experiment, as well as to determine whether the data is consistent in multiple trials, a repeatability analysis was performed. This included retesting the sample again under the same conditions. The results for initial and repeatability tests are shown in Table 3-1.

Table 3-1: Initial and repeatability trials for a constrained surface area tree test section with exposed fin (height 2.52 microns) on a glass substrate (complexity 0).

Initial		Repeatability	
CX2.5G0		CX2.5G0	
Coolant In [˚C]	12.5	Coolant In [˚C]	12.5
Coolant Out [˚C]	14.3	Coolant Out [˚C]	14.2
Mass Flow [g/s]	0.066	Mass Flow [g/s]	0.066
ΔH [W]	0.124	ΔH [W]	0.117
P [W]	0.133	P [W]	0.127
Error [%]	7.10%	Error [%]	8.12%

Table 3-1 shows the power input, P [W], from the power supply in Watts, as well as the outflow temperature of the coolant gas exiting from the heat sink, and the change in enthalpy, ΔH [W], of the coolant gas in Watts. The percent error between the change in enthalpy of the coolant gas and the power supply input is also shown. Notice that the error between the change in enthalpy and the power input is no greater than 10%, which agreed with literature (Hart and da Silva, 2010). Notice also the small difference between the data obtained in the initial and repeatability trials, particularly for the power input, which is well within the calculated statistical uncertainty, or error, of each data point (Appendix B). Therefore, based on all of this, it was concluded that the experimental methodology provides a valid measure of cooling performance.

During the experiment, two important inputs needed to be set including the inlet coolant temperature and the coolant mass flow rate. It was desirable that the inlet temperature should be as low as possible to maximize heat dissipation in the system. This inlet temperature was limited by the cooling in the chiller bath, and was approximately 12 ˚C. The mass flow rate, however, did not have the same limitation, and could be set to any value between 0-2 liters/minute. Due to the type of flow meter used, the error of the

flow measurement depended on the mass flow rate; therefore an error study was conducted in order to determine a suitable mass flow rate setting for the experiment. A plot of the error in the measure of change in enthalpy vs. the measured mass flow rate is shown in Figure 3-4. The so-called "error" is based on the measured statistical uncertainty (Appendix B) associated with the change in enthalpy of the coolant gas to account for the uncertainty of the measuring devices: these included the thermocouples for measuring temperature and the flow meter for measuring mass flow rate. The analysis is based on Eq. 3-1, and Appendix B. The curves shown in Figure 3-4 are constant enthalpy curves. This allows for the plot of mass flow rate as a function of the error.

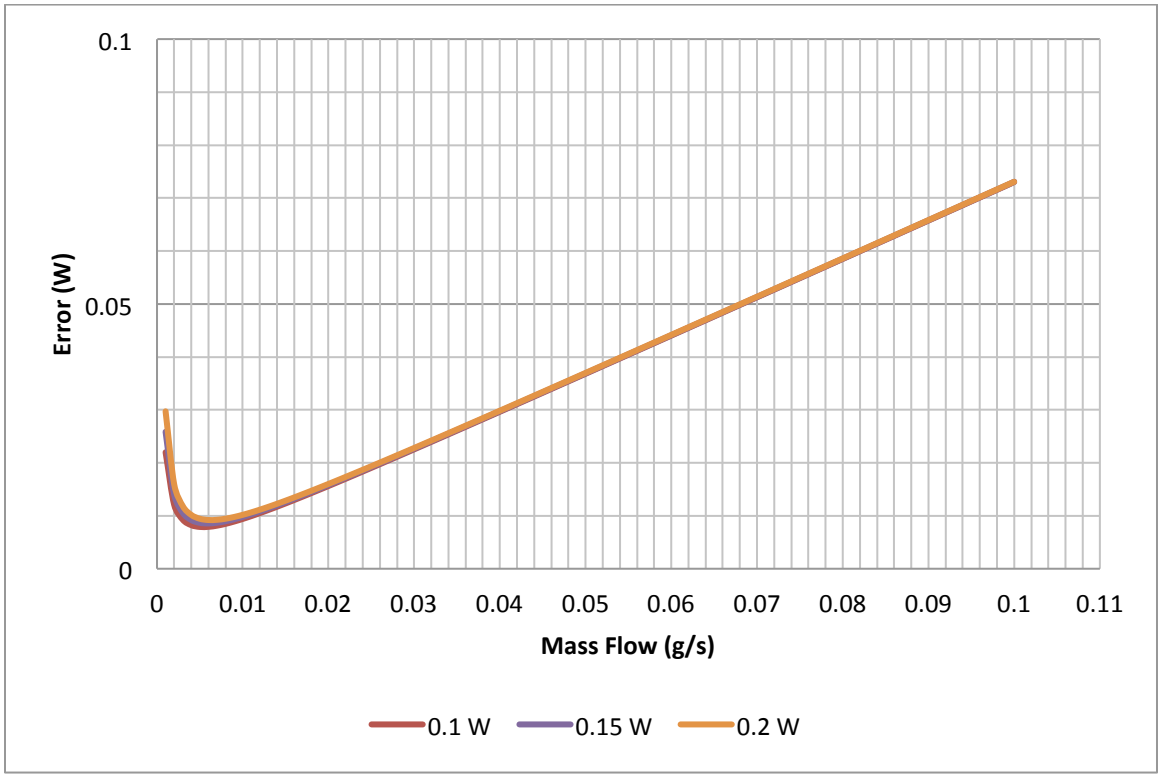

Figure 3-4: Plot of the error in change in enthalpy vs. mass flow rate.

Notice in Figure 3-4 that there exists a minimized error at a mass flow rate of 0.006 grams/second. This is because to the left of the minimum, the change in temperature of the coolant gas begins to dominate the error, while to the right of the minimum the mass flow rate begins to dominate the error. Experimentally, this proved to be too low of a flow rate for a meaningful measure of cooling performance, and therefore a higher flow rate was selected. The mass flow rate recommended should be approximately 0.030 grams/second. The specific heat of the nitrogen for the inlet coolant temperature was found to be 1.04 J/g-K (Incropera et al., 2006).

Chapter 4 Conclusions and Observations

4.1 Recapitulation

In this chapter, the conclusions regarding the test section fabrication processes, the experimental methodology, and the preliminary test results will be discussed. As stated, these conclusions should provide a framework for experimentally determining whether a correlation exists between the geometric complexity of the constructal trees and the cooling performance of these systems. The results of the experimental assessment may provide practical validation to the original theoretical work (Bejan, 1997b; Bejan, 2000).

4.2 Test Section Fabrication

Five constructal tree complexities were designed as a part of test sections. Multiple test section variants were designed to measure the extent of their effects through experiment; these include varying the surface area and height of the constructal tree, changing the substrate material of each test section, and comparing exposed vs. embedded tree conditions. Glass and silicon substrates were selected for their markedly different thermal properties, as well as their availability in wafers for ease of manufacturing. Copper was selected as the constructal tree material because of its good thermal properties. The test sections were fabricated by comparing a variety of techniques: photolithography, reactive ion etching, electroplating, thermal evaporation, sectioning of the test sections into the final 1 cm^2 dimensions, and application of PDMS. The following are important conclusions regarding the test section fabrication methods:

- Use of a viscous photoresist will allow for thick-walled layers to be deposited accurately with a single coat. The thick walls are necessary in order to ensure a proper lift-off process. The use of a release agent like Omni coat will facilitate this process as the photoresist is easily removed from the substrate. Furthermore, proper substrate

cleaning will enhance the adhesion of the resist to the surface of the substrate (Lorenz et al., 1997; Zhang et al., 2001; Song and Ajmera, 2003; Microchem Corp: Omni Coat, 2009).

- Thermal evaporation is a more easily controllable and consistent method for depositing the constructal trees than electroplating. It is more apparent that this is the case when varying the thickness of the trees is desired (Andricacos et al., 1998; ASM: Plating, 2002; ASM: Vacuum coating, 2002; Kurt J. Lesker Company, 2009). The final deposition quality is also better in considering Figure 2-7 vs. Figure 2-8.
- It is possible to embed the fin into the substrate in order to increase the surface area of conducting path in contact with the substrate. This requires an added step of etching the substrate before metal deposition occurs.
- PDMS is an easily moldable material that can be used to insulate these types of test sections to provide for a purely conduction heat transfer performance assessment.

4.3 Experimental Procedure

The experiment based on literature was successfully custom assembled to accommodate the test sections and to allow them to be accurately evaluated. A set-point power supply was used to apply a uniform heat input to each of the test sections. Chilled nitrogen gas was used in the system to create a heat sink. Parameters such as mass flow rate, and inflow and outflow temperature of the gas were measured to calculate the change in enthalpy of the coolant gas to quantify heat losses from the system to ensure experimental accuracy. The following are important conclusions regarding the experimental methodology:

- In order to minimize heat losses during the experiment, sufficient insulation should be applied to the heater. Furthermore, during operation of the experiment, the system should be maintained at ambient temperature while coolant gas impinges on the heat sink. This method is recommended as a means to reduce ambient heat loss and

improve the data point precision, accuracy and repeatability, as recommended (Hart and da Silva, 2010).

- Measuring the change in enthalpy of the coolant gas as it flows into and out of the heat sink area will help to verify that heat losses are minimal. It is recommended that the change in enthalpy not exceed an error of 10% in comparison to the power dissipated by the power supply to ensure minimal heat losses.
- Another very important consideration observed in the experiment is the reduction of contact resistant between the heater and the substrate surface. Proper resolution of this consideration will help to ensure accurate results. It is recommended that a high conductivity thermal paste be used, as well as a means for applying pressure on the test section to reduce any delaminating between the heater and substrate surfaces.
- Performing an error analysis (Figure 3-4) using the accuracy of the measuring equipment as a basis is an important tool for minimizing the error in the experiment. It is also useful for selecting the ideal experimental settings, and potentially improving the accuracy in any trends that may be observed in the obtained data. For this experiment, a mass flow rate of 0.030 grams/second and an inlet coolant temperature of approximately 12 ˚C are recommended. This is to minimize error, to provide sufficient cooling to ensure measurable heat dissipation, and to decrease the likelihood of the formation of condensation within the system.

4.4 Performance Evaluation

The experimental methodology was refined to provide a meaningful and accurate evaluation of cooling performance, and has been validated based on multiple trials in this study and others (Hart and da Silva, 2010). Based on the inputs discussed in Chapter 3 of this report, typical wattages observed during trials have been in the range of 0.1-0.2 Watts, and typical heat losses indicated by the change in enthalpy of the coolant gas are approximately 10% or less. With these observations in mind, the next step in this study is

to run the experiment for each of the fabricated test sections to collect measured data points for each test section. The goal should be to measure the steady state heat dissipation of each test section, and to determine whether the data indicates whether a correlation exists between cooling performance and constructal tree complexity. This should provide a basis for providing any experimental validation to theoretical work (Bejan, 1997a; Bejan, 2000).

Appendix A

Nomenclature

Variables

ϕ - Normalized volume (ratio of volume of conducting pathway to substrate)

$\acute{k}$ - Normalized material thermal conductivity (ratio of thermal conductivity of conducting path to thermal conductivity of substrate)

δ - Denotes value associated with uncertainty or accuracy of parameter

$\dot{m}$ - Mass flow rate (g/s)

c_p - Specific heat (J/g-K)

T - Temperature (˚C)

Q - Heat dissipation (W)

K - Path construct

L - Constructal path length (mm)

W - Constructal path width (mm)

V - Voltage (V)

I - Current (Amps)

P - Power (W)

$\dot{Q}$ - Change in enthalpy (W)

Subscripts

In - Denotes inlet temperature of coolant

Out - Denotes outlet or exit temperature of coolant

Appendix B

Uncertainty Analysis

The uncertainty analysis is a statistical analysis based on standardized techniques recommended by literature (Morgan and Henrion, 1990; Stern et al., 1999; Coleman and Steele, 1999; ASME Standards: PTC 19.1, 2006). Calculations of the systematic uncertainty and the random uncertainty are made and correspond to calculated values based on the specified accuracy of the measurement equipment using the governing equation for each data point, and the data sets collected in the experiment, respectively (Coleman and Steele, 1999). The governing equations for each data point corresponding to power input and change in enthalpy are listed in Equations B-1 and B-2, respectively (Incropera et al., 2006).

$$P = VI \qquad \text{(Eq. B-1)}$$

$$\dot{Q} = \dot{m}c_p(T_{out} - T_{in}) \qquad \text{(Eq. B-2)}$$

Where P is the power in Watts, V is the voltage, I is the current, $\dot{Q}$ is the change in enthalpy in watts, $\dot{m}$ is the gas mass flow rate, c_p is the specific heat of nitrogen, T_{out} is the outflow temperature of nitrogen and T_{in} is the inflow temperature of nitrogen (Incropera et al., 2006). The total uncertainty combines systematic and random uncertainty and is based on a statistical uncertainty analysis using a 95% confidence interval, in which each of the measured parameters such as temperature, voltage, current, and mass flow rate are included. Model equations for the systematic uncertainty and random uncertainty are shown in Equations B-3 and B-4, respectively (ASME Standards: PTC 19.1, 2006).

$$\delta S = \sqrt{\left(\frac{\partial S}{\partial n_1}\delta n_1\right)^2 + \left(\frac{\partial S}{\partial n_2}\delta n_2\right)^2 + \cdots + \left(\frac{\partial S}{\partial n_i}\delta n_i\right)^2} \quad \text{(Eq. B-3)}$$

$$\delta R = \sqrt{\frac{\sum_{i=1}^{m}(x_i-\mu)^2}{m-1}} \quad \text{(Eq. B-4)}$$

Equation B-3 calculates a total variance, and the root of this quantity is the standard deviation, which would correspond to the systematic uncertainty of each data point. The partial derivatives correspond to each measured parameter, and the value of δn_i corresponds to the accuracy of that particular measurement device. Each quantity squared corresponds to the variance associated with the measurement device. Equation B-4 is based on calculating the population standard deviation of the initial and repeatability data points combined, where m is the number of data points (m = 2 for this experiment), x_i is the value of the i^{th} data point, and μ is the population average. The root sum square of the systematic and random uncertainties provides the total uncertainty associated with each data point (ASME Standards: PTC 19.1, 2006).

Glossary

Bifurcation - Occurs when a path branches off at a point into multiple smaller paths resembling the original path geometry.

Conducting pathway - A high thermal conductivity material deposited on a substrate that acts as an extended surface to enhance heat transfer in the system.

Constructal theory - The concept of building upon a base or first order geometry by adding higher order constructs resembling the same geometry to create more complex networks or patterns.

Constructal tree - A predetermined distribution of conducting path material that bifurcates into various path constructs, whose geometry is dictated by constructal theory, to resemble a tree shape.

Electroplating - A thin metal deposition process involving the deposition of a metal onto another surface by a process similar to electrolysis.

Embedded fin - A conducting pathway that is deposited into an etched channel in the top surface of the substrate, acting as an "embedded" pathway.

Exposed fin - A conducting pathway that is deposited on the top surface of the substrate, acting as an extended surface, or fin.

Heat generating volume - A volume, or in this experiment a substrate, that uniformly dissipates heat.

Heat sink - An area that serves to "sink" heat or that facilitates the removal of heat from the system.

Omni coat - A polymer-based material which acts as a release layer to facilitate the removal of photoresist.

Photolithography - The process of using photoresist to create small-scale geometries, using either an electron beam or a patterned mask and electromagnetic radiation, on a substrate for use in numerous applications.

Photoresist - A light reactive material which cures when energy is input in the form of high intensity electromagnetic radiation, creating various small-scale geometries for numerous applications if using a mask.

Polydimethyl siloxane (PDMS) - A silicone-based epoxy which, when mixed, cures into an elastomer having a low thermal conductivity and serves to remove the convective effects on the surface of the test section in this experiment.

Profilometer - A device that applies a small force with a needle and traverses a distance to measure the displacement of the needle over said distance.

Reactive Ion Etching - A process which bombards a surface with unstable gas molecules, ionized using an alternating electromagnetic field, to react with the surface atoms to effectively “etch” the surface.

Substrate - A thin rectangular volume that, in this experiment, simulates a heat generating volume and supports a conducting pathway on or in its top surface.

Test section - A completed sample used in the experiment containing a substrate, a deposited conducting pathway, and a sealing layer of PDMS.

Thermal evaporation - A thin metal deposition process, occurring in a vacuum chamber, that uses low voltage current to evaporate metal and condensing it onto a surface.

Thin metal deposition - The process of depositing a metal at very slow deposition rates by means of a number of techniques.

References

Alebrahim, A. and Bejan, A. (1999). Constructal trees of circular fins for conductive and convective heat transfer. International Journal of Heat and Mass Transfer, vol. 42, no. 19, pp. 3585-3597.

Almogbel, M. & Bejan, A. (2000). Constructal t-shaped fins. International Journal of Heat and Mass Transfer, vol. 43, no. 12, pp. 2101-2115.

Almogbel, M., & Bejan, A. (2001). Constructal optimization of nonuniformly distributed tree-shaped flow structures for conduction. International Journal of Heat and Mass Transfer, Vol. 44, pp. 4185-4194.

Andricacos, P. C., Uzoh, C., & Dukovic, J. O. (1998). Damascene copper electroplating for chip interconnections. IBM Journal of Research and Development, Vol. 42, No. 5, pp. 567-574.

ASTM 281: Practice for preparation of copper and copper-base alloys for electroplating and conversion coatings . (2002). In ASM (Ed.), ASM Handbook. ASM International.

Bejan, A. (1997a). Advanced engineering thermodynamics (Second ed.). New York: John Wiley & Sons, Inc.

Bejan, A. (1997b). Constructal-theory network of conducting paths for cooling heat generating volumes. International Journal of Heat Transfer, Vol. 40, pp. 799-816.

Bejan, A. (1997c). Constructal tree network for fluid flow between a finite-size volume and one source or sink. Revue Generale De Thermique, Vol. 36, No. 8, pp. 592-604.

Bejan, A., Ledezma, G. A. & M. R. Errera (1997). Constructal tree networks for heat transfer. Journal of Applied Physics, vol. 82, no. 1, pp. 89-100.

Bejan, A. & Dan, N. (1999). Constructal trees of convective fins. Journal of Heat Transfer-Transactions of the Asme, Vol. 121, No. 3, pp. 675-682.

Bejan, A. (2000). Shape and structure: From engineering to nature, Cambridge: Cambridge University Press.

Boucher, J. N., & Bajune, D. E. (1997). U.S. Patent No. 387,364. Washington, DC: U.S. Patent and Trademark Office.
Dicing Saw

Brignoni, L. A. & Garimella, S. V. (1999). Experimental optimization of confined air jet impingement on a pin fin heat sink, IEEE Transactions on Components and Packaging Technologies, Vol. 22, No. 3, pp. 399-404.

BYU. (2009). RIE Etching. Retrieved 2009, from http://cleanroom.byu.edu/rie_etching.phtml

Callen, H. B. (1985). Thermodynamics and an Introduction to Thermostatistics. United States: Wiley.

Change-Yen, D. A., Eich, R. K., & Gale, B. K. (2005). A Monolithic PDMS Waveguide System Fabricated. Journal of Lightwave Technology, Vol. 23, No. 6.

Chen, G. (2005). Nanoscale energy transport and conversion. New York: Oxford Press University.

Chiang, K. N, Chou, C. Y., Yuan, C., & Wu, C. C. (2005). Numerical Simulation of The Mechanical Properties of Nanoscale Metal Clusters Using The Atomistic-Continuum Mechanics Method. European Nano Systems 2005, pp. 121-125.

Chung, D. D. L. (2001). Thermal interface materials. Journal of Materials Engineering and Performance, Vol. 10, No. 1, pp. 56-59.

Coleman, H. W. & Steele, W. G. (1999). Experimentation and Uncertainty Analysis for Engineers. (2nd Ed.) New York: John Wiley and Sons.

Culham, J. R. & Muzychka, Y. S. (2001). Optimization of plate fin heat sinks using entropy generation minimization. IEEE Transactions on Components and Packaging Technologies, Vol. 24, No. 2, pp. 159-165.

Dettinger, P. M., Clift, W. M., & Goods, S. H. (2002). Removal of SU-8 photoresist for thick film applications. Microelectronic Engineering, Vol. 61, pp. 993-1000.

Dubin, V. M., Morales, G., Ryu, C., & Wong, S. S. (1997). Microstructure and Mechanical Properties of Electroplated Cu Films for Damascene ULSI Metallization. Materials Research Society.

Federov, A. G. & Viskanta, R. (2000). Three-dimensional conjugate heat transfer in the microchannel heat sink for electronic packaging. International Journal of Heat and Mass Transfer, Vol. 43, pp. 399-415.

Gersborg-Hansen, A., Bendsoe, M. P. & Sigmund, O. (2006). “Topology optimization of heat conduction problems using the finite volume method.” pp. 251-259.

Gosselin, L. & Bejan, A. (2004). Constructal heat trees at micro and nanoscales, Journal of Applied Physics, Vol. 96, No. 10, pp. 5852-5859.

Gosselin, L., & Mathieu-Potvin, F. (2007). Optimal conduction pathways for cooling a heat generating bodies: A comparison excercise. International Journal of Heat and Mass Transfer, Vol. 50, pp. 2996-3006.

Hart, R.A. & Da Silva, A. K. (2010). Experimental thermal-hydraulic evaluation of constructal microfluidic structures under fully constrained conditions, submitted for review to the International Journal of Heat and Mass Transfer in 2010.

Incropera, F. P., Dewitt, D. P., Bergman, T. L., & Lavine, A. S. (2006). The Fundamentals of Heat and Mass Transfer (Sixth ed.). New York, NY: John Wiley and Sons, Inc.

Jacob Baker, R. (2008). Cmos circuit design, layout, and simulation. New York: John Wiley & Sons, Inc.

Kobayashi, M. H., Pedro, H. C., Coimbra, C. F. M. & A. K. da Silva (2009). Formal evolutionary development of low entropy dendritic thermal systems. Journal of Thermophysics and Heat Transfer, Vol. 23, No. 4, pp. 822-827.

Kurt J. Lesker Company. (2009). Deposition techniques. Retrieved April 1, 2009, from http://www.lesker.com/newweb/Technical_Info/MaterialDeposition.cfm?section=materials&init=skip

Ledezma, G. A., & Bejan, A. (1998). Constructal three-dimensional trees for conduction between a volume and one point. Journal of Heat Transfer, Vol. 120, pp. 977-984.

Li, Q., Steven, G. P., Xie, Y. M. & Querin, O. M. (2004). Evolutionary topology optimization for temperature reduction of heat conducting fields, International Journal of Heat and Mass Transfer, vol. 47, no. 23, pp. 5071-5083.

Lorenz, H., Despont, M., Farhni, N., LaBianca, N., Renaud, P., & Vettiger, P. (1997). SU-8: a low-cost negative resist for MEMS. Journal of Micromechanics and Microengineering, Vol. 7, No. 3.

Magill, P. (2010, March 18). Active heat removal cools electronics hot spots. Electronics Design, Strategy and News.

Microchem Corp Technical Resources. (2009). Retrieved 2009, from http://www.microchem.com/

Microchem Corp. (2009). Omni Coat (Microchem Corp, Ed.).

Microchem Corp. (Ed.). (2009, April 1). SU-8 2000 permanent epoxy negative photoresist processing guidelines. Retrieved from http://www.microchem.com/products/pdf/SU-82000DataSheet2000_5thru2015Ver4.pdf

Mills, A. E. (1999). Heat Transfer (Second ed.). New York: Prentice Hall Literature.

MIT. (2010). Material Properties Database. Retrieved 2010, from http://www.mit.edu/~6.777/matprops/pdms.htm

Moore, G. E. (1965). Cramming more components onto integrated circuits. Electronics, Vol. 38, No. 8.

Morgan, M. G. & Henrion, M. (1990). Uncertainty: A Guide to Dealing With Uncertainty in Quantitative Risk and Policy Analysis. New York: Cambridge University Press.

Murray, C. D (1926). The Physiological Principle of Minimum Work. I. The Vascular System and the Cost of Blood Volume. Proceedings of the National Academy of Sciences of the United States of America, Vol. 12, No. 3, pp. 207-214.

NIST. (2009). NIST reference fluid thermodynamic and transport properties. (retreived from http://www.nist.gov/ 2009)

Omega Engineering Inc. (2009). Digital Linear Power Supplies.

Omega Engineering Inc. (2009). Epoxies and Thermally Conductive Pastes.

Omega Engineering Inc. (2009). Introduction to Flow Meters. Retrieved 2009, from http://www.omega.com/prodinfo/flowmeters.html

Omega Engineering Inc. (2009). Thermocouples and thermocouple probes. Retrieved 2009, from http://www.omega.com/thermocouples.html

Papra, A., Bernard, A., Juncker, D., Larsen, N. B., Michael, B. & Delamarche, E. (2001). Microfluidic networks made of poly(dimethylsiloxane), Si,and Au coated with polyethylene glycol for patterning proteins onto surfaces. Langmuir, Vol. 17, pp. 4090–4095.

PTC 19.1: Test Uncertainty. (2005). In ASME (Ed.), *ASME Standards* (pp. 5-42).

Plating and Electroplating. (2002). In B. J. Durkin & L. M. Weisenberger (Eds.), ASM Handbook: Vol. 5. Surface Engineering. ASM International.

Pop, E., Sinha, S. & Goodson, K. E. (2006). Heat generation and transport in nanometer-scale transistors. Proceedings of the IEEE, vol. 94, no. 8, pp. 1587-1601.

Ramm, J., Beck, A., Zuger, E., Dommann, A., & Pixley, R. E. (1992). Low-temperature in situ cleaning of silicon wafers with an ultra high vacuum compatible plasma source. Thin Solid Films, Vol. 222, No. 1, pp. 126-131.

Rocha, L. O., Lorente, S., & Bejan, A. (2002). Constructal design for cooling a disc-shaped area by conduction. International Journal of Heat and Mass Transfer, 45, 1643-1652.

Rossnagel, S. M., Cuomo, J. J., & Westwood, W. D. (1990). Reactive Ion Etching. In Handbook of plasma processing technology: fundamentals, etching, deposition and surface interactions (pp. 196-230). Norwich, NY: Noyes Publishing.

Schaller, R. R. (1997). Moore's law: past, present and future. Spectrum, IEEE. Vol. 34, No. 6.

Schmidt, P. S., Ezekoye, O. A., Howell, J. R., & Baker, D. K. (2006). Thermodynamics. United States: Wiley.

Song, I., & Ajmera, P. K. (2003). Use of a photoresist sacrificial layer with SU-8 electroplating mould in MEMS fabrication. Journal of Micromechanics and Microengineering, Vol. 13, No. 6.

Stern, F., Muste, M., Beninati, M. L., & Eichinger, W. E. (1999). Summary of Experimental Uncertainty Assessment Methodology with Example. Iowa Institute of Hydraulic Research. IIHR Technical Report No. 406.

Thermo Scientific. (2009). NESLAB RTE and EX Series (Thermo Scientific, Ed.). Thermo Scientific.

Vacuum and controlled atmosphere coating. (2002). Rhode, S. L. (Eds.), ASM Handbook: Vol. 5. Surface Engineering. ASM International.

Webb, R. L. & Kim, N. H. (2005). Principles of enhanced heat transfer. New York: Taylor & Francis.

West, G. B., and Brown, J. H. (1997). A General Model for the Origin of Allometric Scaling Laws in Biology. Science, Vol. 276, No. 5309, pp. 122-126.

Williams, J. D., & Wang, W. (2004). Study on the postbaking process and the effects on UV lithography of high aspect ratio SU-8 microstructures. Society of Photo-Optical Instrumentation Engineers, Vol. 3.

Zhang, J., Tan, K. L., Hong, G. D., Yang, L. J., & Gong, H. Q. (2001). Polymerization optimization of SU-8 photoresist and its applications in microfluidic systems and MEMS. Journal of Micromechanics and Microengineering, Vol. 11, No. 1.

Zhou, Z., & Woods, E. (2009). Plasma Etching. Georgia Institute of Technology.

Vita

Sean Michael Berg was born in San Antonio, Texas on May 12, 1986. He attended the Design and Technology Academy, an engineering and computers magnet school, at Roosevelt High School in San Antonio. He later enrolled at The University of Texas at Austin in the spring of 2006. As an undergraduate, he gained valuable industry experience by completing a three-semester co-op with Toyota Motor Manufacturing, TX in San Antonio, Texas. He decided to gain experience in education and teaching by working as a math instructor at Sylvan Learning Center, and as an engineering tutor at the Cockrell School of Engineering. He later worked as a teaching assistant as a graduate in the thermal-fluids department at The University of Texas at Austin. He received the degree of Bachelor of Science in Mechanical Engineering from The University of Texas at Austin in December 2008. In January 2009, he entered the Graduate School at The University of Texas at Austin in Mechanical Engineering.

Permanent address: 22349 Old Fossil Rd, San Antonio, Texas 78261

This report was typed by Sean Michael Berg.